

Modal Folding: Discovering Smooth Folding Patterns for Sheet Materials using Strain-Space Modes

Supplementary Material

Pengbin Tang

ETH Zürich
Switzerland

Université de Montréal
Canada
petang@ethz.ch

Ronan Hinchet

ETH Zürich
Switzerland

ronan.hinchet@srl.ethz.ch

Roi Poranne

ETH Zürich
Switzerland

University of Haifa
Israel
roi.poranne@inf.ethz.ch

Bernhard Thomaszewski

ETH Zürich
Switzerland
bthomasz@inf.ethz.ch

Stelian Coros

ETH Zürich
Switzerland
stelian@inf.ethz.ch

CCS CONCEPTS

- Applied computing → Computer-aided design; • Computing methodologies → Modeling and simulation.

KEYWORDS

Nonlinear Modal Analysis, Computational Design, Folding, Origami

ACM Reference Format:

Pengbin Tang, Ronan Hinchet, Roi Poranne, Bernhard Thomaszewski, and Stelian Coros. 2024. Modal Folding: Discovering Smooth Folding Patterns for Sheet Materials using Strain-Space Modes Supplementary Material. In *Special Interest Group on Computer Graphics and Interactive Techniques Conference Conference Papers '24 (SIGGRAPH Conference Papers '24), July 27-August 1, 2024, Denver, CO, USA*. ACM, New York, NY, USA, 4 pages. <https://doi.org/10.1145/3641519.3657401>

1 THIN SHEET MECHANICS

We model the mechanics of thin sheets using discrete shell models [Gingold et al. 2004; Grinspun et al. 2003] represented as triangle meshes. Let $\mathbf{x} \in \mathbb{R}^{3n}$ and $\mathbf{X} \in \mathbb{R}^{3n}$ denote vertex positions for deformed and reference configurations, respectively. The discrete shell energy $W = W^{\mathcal{M}} + W^{\mathcal{B}}$ consists of a membrane term $W^{\mathcal{M}}$ measuring in-plane deformation and a bending term $W^{\mathcal{B}}$ that penalizes changes in curvature. For the membrane energy, we combine the St. Venant-Kirchhoff material model with linear triangle finite elements. The per-triangle energy is given as

$$W^{\mathcal{M}} = A \left(\mu \text{tr}(\mathbf{E}^T \mathbf{E}) + \frac{\lambda}{2} \text{tr}^2(\mathbf{E}) \right), \quad (1)$$

Permission to make digital or hard copies of all or part of this work for personal or classroom use is granted without fee provided that copies are not made or distributed for profit or commercial advantage and that copies bear this notice and the full citation on the first page. Copyrights for components of this work owned by others than the author(s) must be honored. Abstracting with credit is permitted. To copy otherwise, or republish, to post on servers or to redistribute to lists, requires prior specific permission and/or a fee. Request permissions from permissions@acm.org.

SIGGRAPH Conference Papers '24, July 27-August 1, 2024, Denver, CO, USA
© 2024 Copyright held by the owner/author(s). Publication rights licensed to ACM.
ACM ISBN 979-8-4007-0525-0/24/07...\$15.00
<https://doi.org/10.1145/3641519.3657401>

where A is the area of the triangle in its reference configuration, $\mathbf{E} = (\mathbf{F}^T \mathbf{F} - \mathbf{I})/2$ is the Green-Lagrange strain with the deformation gradient \mathbf{F} , while μ and λ are the Lamé parameters.

We explore two options for the bending energy. The first one is the hinge energy proposed by Grinspun et al. [2003],

$$W^{\mathcal{H}} = \alpha (\theta - \bar{\theta})^2, \quad (2)$$

where θ and $\bar{\theta}$ are dihedral angles between two edge-adjacent triangles in their deformed and undeformed configurations, and $\alpha = \|\vec{e}\|/\bar{h}_e$, where \bar{h}_e is a third of the mean triangle heights incident to the edge. While the hinge-based model penalizes changes in mean curvature, more precise control over curvature in different directions is obtained when using discrete shape operators [Grinspun et al. 2006]. We follow Gingold et al. [2004] and use a discretization of the shape operator based on a given triangle and its three edge-adjacent neighbor triangles. Using this model, per-triangle bending strains $\Delta S = S - \bar{S}$ are computed as the difference between shape operators in the deformed (S) and undeformed (\bar{S}) configurations. These bending strains characterize the curvature of a given triangle element and can thus be used to model direction-dependent materials. We focus on orthotropic materials, which can be used to describe, e.g., textiles, cardboard, and reinforced plastics. The per-triangle bending energy of an orthotropic thin shell [Garg et al. 2007] is given as

$$W^S = c(Y^0 \Delta S_{00}^2 + Y^1 \Delta S_{11}^2 + 2Y^{01} \Delta S_{00} \Delta S_{11}) + 2\eta G^{01} \Delta S_{01}^2, \quad (3)$$

where Y^0 and Y^1 are Young's moduli along two orthogonal material directions, ν_{01} and ν_{10} are corresponding Poisson's ratios, and G^{01} is the shear modulus. Furthermore, we use the shorthands $Y^{01} = \nu_{01} Y^1 = \nu_{10} Y^0$ and $c = \eta Y^0 Y^1 / (Y^0 Y^1 - Y^{01}) Y^{01}$, where $\eta = Ah^3/12$ is a geometry factor depending on the material's thickness h . For the special case of isotropic materials, we set $Y^0 = Y^1 = 2(1+\nu)G^{01} = Y^{01}/\nu$.

2 INVERSE DESIGN

To implement the inverse folding problem described in Sec. 4.4 of the main document, we use the squared distance $d_i^2 = \|\mathbf{x}_i(\mathbf{p}) - \mathbf{x}_s\|^2 - r^2$ of a given vertex \mathbf{x}_i to the center of a sphere \mathbf{x}_s with

radius r . We then formulate a constraint optimization problem as

$$\arg \min_{\mathbf{p}} \sum_i T_i(\mathbf{p}) = \begin{cases} d_i^2 & d_i^2 > 0 \\ 0 & d_i^2 \leq 0 \end{cases} \quad \text{s.t. } \mathbf{f}(\mathbf{p}) = \mathbf{0}, \quad (4)$$

where the design parameters $\mathbf{p} = [\mathbf{c}, \mathbf{r}]^\top$ include the modal coefficients \mathbf{c} for strain-space modes and the parameters for rigid transformations \mathbf{r} of the sheet. The constraint $\mathbf{f}(\mathbf{p}) = \mathbf{0}$ requires the sheet to be at equilibrium. We convert this optimization problem into an unconstrained minimization problem using the implicit relation between \mathbf{x} and \mathbf{p} given by the static equilibrium constraints,

$$\frac{d\mathbf{f}}{d\mathbf{p}} = \frac{\partial \mathbf{f}}{\partial \mathbf{x}} \frac{d\mathbf{x}}{d\mathbf{p}} + \frac{\partial \mathbf{f}}{\partial \mathbf{p}} = \mathbf{0}. \quad (5)$$

from which we obtain the sensitivity matrix as

$$\frac{d\mathbf{x}}{d\mathbf{p}} = -\frac{\partial \mathbf{f}^{-1}}{\partial \mathbf{x}} \frac{\partial \mathbf{f}}{\partial \mathbf{p}}. \quad (6)$$

We eliminate a total of 6 degrees of freedom from 3 vertices to ensure that $\partial \mathbf{f} / \partial \mathbf{x}$ is non-singular and compute the objective gradient as

$$\frac{dT}{d\mathbf{p}} = -\left(\frac{\partial \mathbf{f}^{-1}}{\partial \mathbf{x}} \frac{\partial \mathbf{f}}{\partial \mathbf{p}}\right) \frac{\partial T}{\partial \mathbf{x}} + \frac{\partial T}{\partial \mathbf{p}}. \quad (7)$$

To compute the action of the inverse force Jacobian, we solve a single linear system. We use the resulting gradient with L-BFGS [Liu and Nocedal 1989] to find parameters that minimize the design objective.

3 MATERIAL PROPERTIES

Our method builds on a physics-based thin shell model and, consequently, strain-space modes change as a function of the sheet's mechanical properties.

Isotropic Materials. Modifying Young's modulus for isotropic materials will not alter modal shapes since stretching and bending energies scale in equal proportions. The thickness of the sheet, however, offers a means of controlling the ratio between stretching and bending stiffness: stretching resistance scales linearly with respect to thickness whereas bending resistance is a cubic function of thickness. In the example shown in Fig. 1, we successively decrease the thickness of a square sheet and study the resulting change in modal shapes. For a thickness-to-width ratio of 0.5%, we observe smooth folds. Reducing the ratio down to 0.005% leads to increasingly sharper folds and creases. We further observe that a decrease in thickness generally reduces in-plane deformations. For the example shown in Fig. 1, the maximum in-plane strains are $4.68e^{-2}$, $2.03e^{-3}$, and $1.16e^{-4}$ for thickness values of 1mm, 0.1mm, and 0.01mm, respectively.

Orthotropic Materials. Triangle-based discrete shell elements offer precise control over the sheet's response to curvature in any material direction. To illustrate this effect, we compare isotropic hinge-based elements, isotropic triangle-based bending elements, and orthotropic triangle-based bending elements. For both isotropic elements, we set Young's modulus to $Y = 4MPa$ and use a Poisson's ratio of $\nu = 0.2$. For orthotropic elements, we set $Y_0 = Y/10$, $Y_1 = Y$, $v_{01} = \nu$, and $G_{01} = Y/8$, leading to softer bending in the material's x -direction. We focus on mode 7 as it displays the most salient differences among the above models. As can be seen from Fig. 2, we

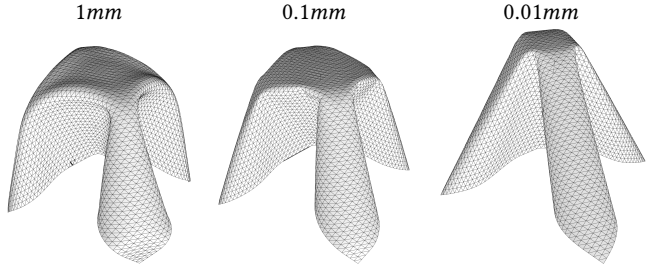


Figure 1: Modes comparison with the decreasing thickness from 1mm to 0.01mm. The modes are in order of 15, 15, and 12 from left to right for their corresponding thicknesses. We can see with a thinner thickness the order of mode will be shifted to lower order and can get sharper creases while folding.

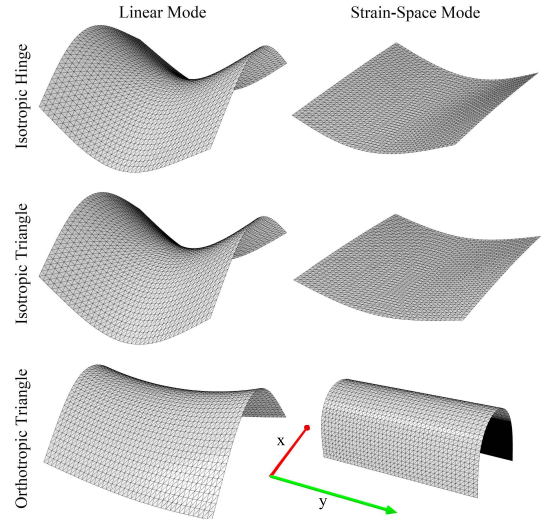


Figure 2: Modes comparison for thin shells with isotropic hinge-based bending, isotropic triangle-based bending, and orthotropic triangle-based bending.

obtain almost identical linear modes for the isotropic models with similar amounts of curvature in two principal directions, whereas the orthotropic model displays significantly more bending in the x -direction. For the corresponding strain space modes, we observe that both isotropic thin shells exhibit similar cylindrical bending in the y -direction. The orthotropic model, in contrast, shows substantial bending in the softer x -direction.

4 DISCRETIZATION EFFECTS

Besides shape and material properties, modes are also affected by discretization. We investigate this dependence with two sets of examples, starting with mesh refinement.

Mesh Refinement. We begin by examining how mesh resolution affects strain-space modes. For low-order modes, we generally find that mesh resolution has little effect on mode shape. An example

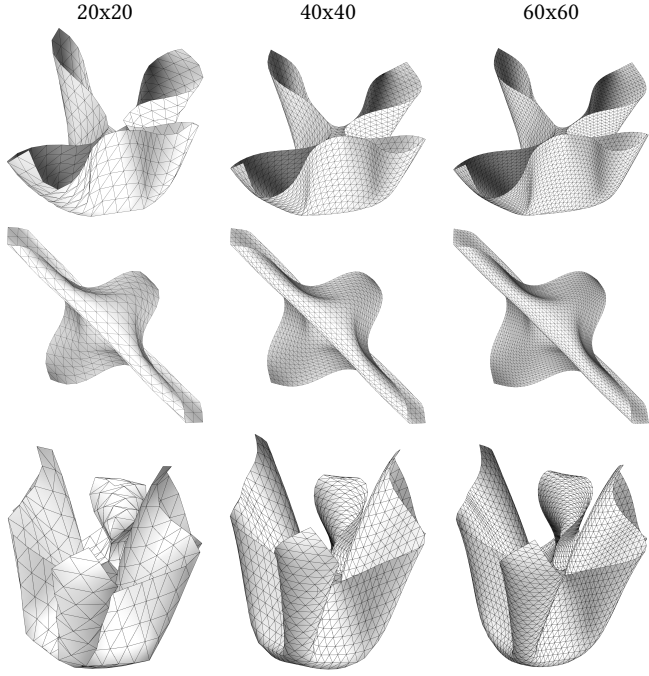


Figure 3: Effect of mesh resolution on mode shape for a square sheet. Modes 15 (top), 20 (middle), and 26 (bottom) are shown for three different resolutions (as indicated).

can be seen in Fig. 3, showing fairly consistent behavior under refinement. Higher order modes can show larger differences if they exhibit features beyond the resolution of coarser meshes.

Symmetry of Discretization. We further investigate the behavior of strain-space modes by altering mesh topology from reflection symmetry to four-fold rotational symmetry. As can be seen from Fig. 4 mesh topology can have a substantial impact on mode shape. This observation is explained by the fact that the underlying mechanical model is not independent of discretization, as bending can only occur along edges. A further observation is that higher mesh symmetry also translates into higher symmetry in modal shapes.

4.1 Extrapolation Range

Extrapolation Range. For any folding mode, extrapolation will ultimately produce self-contact, which is handled by a log-barrier contact potential. Continued actuation leads to increasing compaction which, depending on the mode, can lead to either flat-folded or crumpled configurations, see Fig. 5 for an example.

REFERENCES

- Akash Garg, Eitan Grinspun, Max Wardetzky, and Denis Zorin. 2007. Cubic shells. In *Proceedings of the 2007 ACM SIGGRAPH/Eurographics symposium on Computer animation*. Citeseer, 91–98.
- Yotam Gingold, Adrian Secord, Jefferson Y Han, Eitan Grinspun, and Denis Zorin. 2004. A discrete model for inelastic deformation of thin shells. In *ACM SIGGRAPH/Eurographics symposium on computer animation*. Citeseer.
- Eitan Grinspun, Yotam Gingold, Jason Reisman, and Denis Zorin. 2006. Computing discrete shape operators on general meshes. *Computer Graphics Forum (Eurographics)* 25, 3 (2006), 547–556. <https://doi.org/10.1111/j.1467-8659.2006.00974.x>

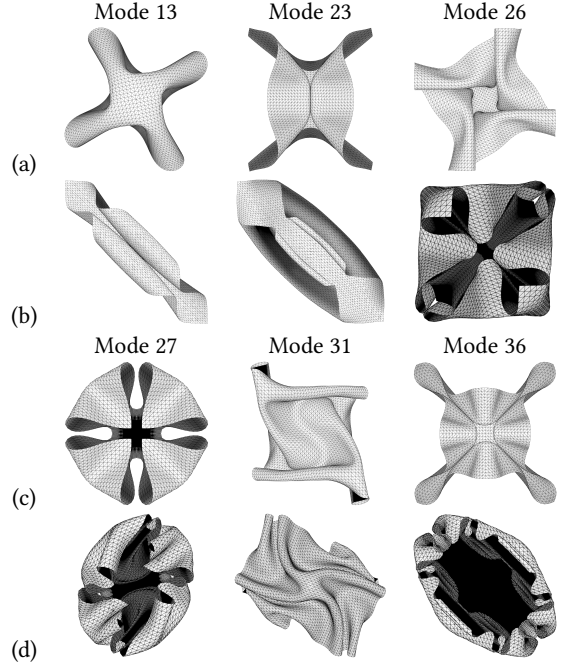


Figure 4: Changing mesh topology for a square sheet from reflection symmetry (b and d) to four-fold rotational symmetry (a and c) yields more symmetric folding patterns for low-order modes.

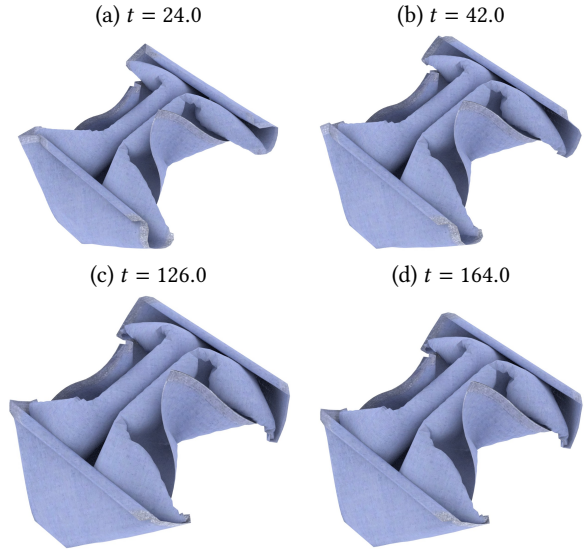


Figure 5: We extrapolate mode 30 of a square sheet. As the extrapolation progresses (a–c), two diagonally opposing tips gradually move toward the center. Upon reaching a certain threshold (c), the contact potential prevents further compaction. Additional extrapolation (d) leads to little visual difference.

Eitan Grinspun, Anil N Hirani, Mathieu Desbrun, and Peter Schröder. 2003. Discrete shells. In *Proceedings of the 2003 ACM SIGGRAPH/Eurographics symposium on Computer animation*. Citeseer, 62–67.

Dong C Liu and Jorge Nocedal. 1989. On the limited memory BFGS method for large scale optimization. *Mathematical programming* 45, 1-3 (1989), 503–528.